ACS OMEGA

http://pubs.acs.org/journal/acsodf

Article

Novel Chemoresistive Sensor for Sensitive Detection of Pb^{2+} Ions Using an Interdigital Gold Electrode Fabricated with a Reduced Graphene Oxide-Based Ion-Imprinted Polymer

Mokgehle R. Letsoalo, Abayneh A. Ambushe, and Messai A. Mamo*

Cite This: *ACS Omega* 2021, 6, 31528−31538

Read Online

ACCESS | Metrics & More | Article Recommendations | Supporting Information

ABSTRACT: This study presents novel chemoresistive reduced graphene oxide−ion-imprinted polymer (IIP−rGO)-based sensors for detection of lead (Pb^{2+}) ions. The ion-imprinted polymer was synthesized by bulk polymerization and modified with a variable amount of rGO incorporated to form an IIP−rGO composite. The amount of rGO in the polymer matrix affected the sensor's relative response, and 1:3 mass ratio produced excellent results, with a consistent trend as the concentration of Pb^{2+} ions increased in the solution. The decrease in relative resistance ($\Delta R/R_o$) followed an exponential decay relationship between the $\Delta R/R_o$ response and the concentration of Pb^{2+} ions in aqueous solutions. After solving the exponential decay function, it is observed that the sensor has the upper limit of $\Delta R/R_o$ >1.7287 μg L^{-1}, and the limit of detection of the sensor is 1.77 μg L^{-1}. A nonimprinted polymer (NIP)-based sensor responded with a low relative resistance of the same magnitude although the concentration was varied. The response ratio of the IIP-based sensor to the NIP-based sensor $(\Delta R/R_o)_{IIP}/(\Delta R/R_o)_{NIP}$ as a function of the concentration of Pb^{2+} ions in the solution shows that the response ratios recorded a maximum of around 22 at 50 μg L^{-1} and then decreased as the concentration increased, following an exponential decay function with the minimum ratio of 2.09 at 200 μg L^{-1} but never read 1. The sensor showed excellent selectivity against the bivalent cations Mn^{2+}, Fe^{2+}, Sn^{2+}, and Ti^{2+}. The sensor was capable of exhibiting 90% $\Delta R/R_o$ response repeatability in a consecutive test.

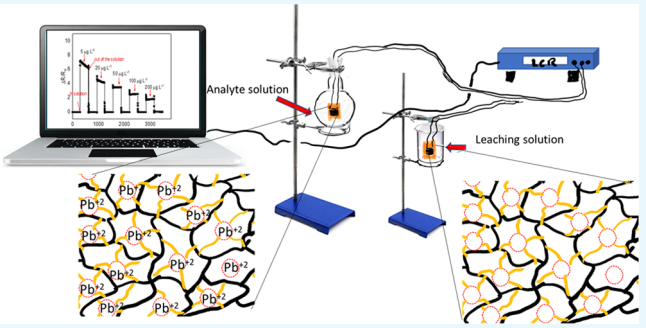

1. INTRODUCTION

Pollution of water by toxic elements that may affect ecosystems and human health is an utmost concern. Humans may indirectly be intoxicated with lead (Pb) through the food chain of soil-to-plant-to-animal-to-human. In contrast, direct exposure may occur through the inhalation of dust and drinking water polluted in the emission source's vicinity.[1] Lead mostly toxifies vital organs such as neurological, reproductive, renal, and gastrointestinal systems even at ultratrace levels.[2] Lead pollution of environmental media (water, soil, air) usually may be influenced by the mismanagement of the byproducts from industrial activities.[3] Lead exists in three different oxidational states, with metallic lead rarely occurring in nature.[4] Pb^{5+} is formed in highly oxidizing conditions, and Pb^{5+} compounds generally do not exist under standard environmental conditions. The Pb^{2+} is the most stable oxidation state that primarily dominates the chemistry of Pb in the environment and is responsible for severe toxicity.[4,5] A significant impact of Pb^{2+} on human health and the ecosystem evoked a fixed maximum permissible level (MPL) to control harmful effects and devise a stringent guideline to curb water pollution.[6] South African water quality and World Health Organization standard water guidelines have recommended 10 μg L^{-1} MPL of Pb^{2+} in drinking water.[7,8] The gradual accumulation and environmental impacts of toxic Pb^{2+} have evoked the need to quantify and monitor Pb^{2+} in the different matrices (water, soil, and sediment) before it accumulates to the level that poses risks.[3]

The most used conventional analytical techniques for the determination of toxic elements in various sample matrices include flame-atomic absorption spectrometry, inductively coupled plasma-mass spectrometry (ICP-MS), inductively coupled plasma-atomic emission spectrometry (ICP-AES), hydride generation-atomic absorption spectrometry, and graphite furnace atomic absorption spectrometry. These techniques have the advantages of high sensitivity and selectivity with some shortcomings such as the expensive cost, requirement of expertise for operation, and time consumption. Moreover, constituents of a sample matrix,

Received: July 25, 2021
Accepted: October 7, 2021
Published: November 16, 2021

such as cations, anions, and particulate matter, may pose spectroscopic and nonspectroscopic interferences, leading to inaccurate determination of the analyte concentration.[9] These conditions of conventional techniques promoted the pressing need to develop ion-imprinted polymer (IIP)-based sensor techniques with recognition cavities to target analyte ions in the presence of matrix components accurately. The establishment of IIP with exceptional sensitivity, selectivity, cost-effectiveness, and ease of operation and maintenance may overcome the drawbacks of conventional techniques. The ion-imprinting technology creates template-shaped three-dimensional active cavities in the polymeric network matrix with predetermined selectivity and high affinity.[5,10] The recognition of the target analyte ion is based on the lock-and-key phenomenon, which holds a universal application of imprinted polymers, owing to the unique features with structural predictability, recognition specificity, simple design, cost-effectiveness, eco-friendliness, and excellent stability.[5,11]

The capability of IIP to target analyte ions from a complex matrix with excellent selectivity has attracted massive attention to develop IIP-fabricated transducers for the detection of Pb^{2+} in water. The agglomerated IIP lacks electrical conductivity and low signal response for target analyte binding, and nontunable surface properties of imprinted polymer layers may limit the efficient performance of IIP.[5,11] However, the use of reduced graphene oxide (rGO) with excellent thermal stability, electrical conductivity, mechanical strength, good electron transport, high specific surface as nanofillers in the polymeric network matrix enhances the performance of IIP.[12] The IIP−rGO formation can be initiated by the interface of functional groups (hydroxyl, carboxyl, and carbonyl) on the surface and rGO on the edge regions with the IIP. Thus, the combined features of rGO and IIP provide a nanocomposite with exceptional features for a sensor-based method.

Electrochemical and optical sensing techniques have been used extensively for the detection of metal ions using chemically modified fabricated sensors not limited to the composites of IIPs.[13−16] These techniques possess attractive advantages such as low-cost instrumentation, excellent sensitivity, good selectivity, and ease of portability for detecting toxic metal ions in various samples.[13] However, our study on the IIP−rGO-fabricated sensor for the chemoresistive detection of Pb^{2+} ions with exceptional efficiency and selectivity is significant and presents a recent innovation in the development of chemical sensing technology. The robustness of the IIP−rGO-based sensor to perform chemoresistive detection due to a change in relative resistance ($\Delta R/R_o$) in response to the rebinding of Pb^{2+} ions on the imprinted cavities of the fabricated sensor. An electronic test device that measures inductance (L), impedance (Z), capacitance (C), and resistance (R), known as an LCR meter, provided compatibility to facilitate the chemoresistive performance of the IIP−rGO-based sensor. This work presents the novel fabrication of a simple, cheap, and fast thin-film chemoresistive sensor coated with IIP−rGO to detect Pb^{2+} in water. The performance parameters such as sensitivity, linearity, precision, accuracy, limit of detection (LOD), and selectivity were optimized using an LCR meter. A nonimprinted polymer (NIP)−rGO-based sensor was established as a control to evaluate the sensor-based method's performance.

2. RESULTS AND DISCUSSION

2.1. Characterization of the Synthesized Material Hybrids. The synthesized material hybrids with unleached IIP, leached IIP, and NIP were characterized using Fourier transform infrared (FTIR) and Raman spectroscopy, powder X-ray diffraction (P-XRD), N_2 adsorption/desorption experiment, scanning electron microscopy (SEM), and transmission electron microscopy (TEM).

2.1.1. Fourier Transform Infrared Spectroscopy Analysis. The FTIR was used to study the chemical structure, surface functional groups, and bonding nature of spectral profiles of unleached IIP and NIP. The spectra are presented in Figure 1a. A close similarity in the chemical structure of unleached IIP and NIP is primarily attributed to the presence of the cross-linking agent used ethylene glycol dimethacrylate (EDGMA).[19] However, slight changes in the absorption shifts and peak intensities were notable. The absorptions at 2985 and 2896 cm^{-1} in the polymeric materials were attributed to aliphatic C−H stretching vibrations of the sp^3 hybrid. The absorptions at 1590 and 1080 cm^{-1} in the unleached IIP and NIP are ascribed to the C═O and C−O stretching bonds, respectively. Similar peaks appeared in the case of unleached IIP; however, the intensities of the peaks at 1157 and 1728 cm^{-1} due to C−O and C═O, respectively, became weaker in the case of unleached IIP (Figure 1a) and the Pb−O peak was not identifiable in the FTIR spectra of IIP; this is mainly because the strong IR absorption by the polymer at low wavelengths overshadowed the Pb−O bond.[20]

2.1.2. Raman Spectroscopy Analysis. Raman spectroscopy was used to study the vibrational properties of GO, rGO, unleached IIP, and NIP. The spectra are presented in Figure 1b,c. The main characteristic peaks on the graphene derivatives of GO and rGO are assigned to the D and G bands located at about 1338 and 1595 cm^{-1} at the GO/rGO Raman spectrum (Figure 1b).[21] A distinct feature of the D and G bands of GO/rGO is the relative intensity ratio (I_D/I_G), which assesses the amorphous sp^3 domain carbon relative to sp^2-bonded carbon atoms. An I_D/I_G from 1.13 of GO to 0.84 of rGO after a synthetic process of rGO suggested a reduction of defects attributed to the fact that the disordered sp^3 amorphous carbon dominated the structure of GO. The spectrum of rGO showed highly ordered and stable sp^2 graphitic carbon, which is strong evidence that GO was significantly reduced to rGO. The Raman shifts of unleached IIP and NIP were compared. Interestingly, the vibration bands at 386 and 558 cm^{-1} of the unleached IIP were due to the presence of Pb−O (Figure 1c inset),[22] and this confirmed the successful incorporation of template ion Pb^{2+} in the polymer matrix of the IIP. These particular Raman shifts were absent in NIP.

2.1.3. Powder X-ray Diffraction Analysis. The P-XRD was used to investigate the structural features of the imprinted polymers and nanocomposites. The diffraction pattern of unleached IIP is presented in Figure 2a, and the deconvoluted peak at $2\theta = 31.5°$ is due to Pb−O;[23] this particular peak was absent in NIP, which confirms the successful incorporation of the template ions (Pb^{2+} ions) in the polymer matrix. This finding complements the result obtained by Raman analysis. The absence of a peak at $2\theta = 31.5°$ in the leached IIP indicates the successful removal of the template ion from IIP (Figure 2c). The P-XRD pattern of rGO (Figure 2d) shows a diffraction angle at $2\theta = 24.8°$ assigned to the (002) plane due to amorphous carbonaceous of rGO with an interlayer spacing

https://doi.org/10.1021/acsomega.1c03955
ACS Omega 2021, 6, 31528−31538

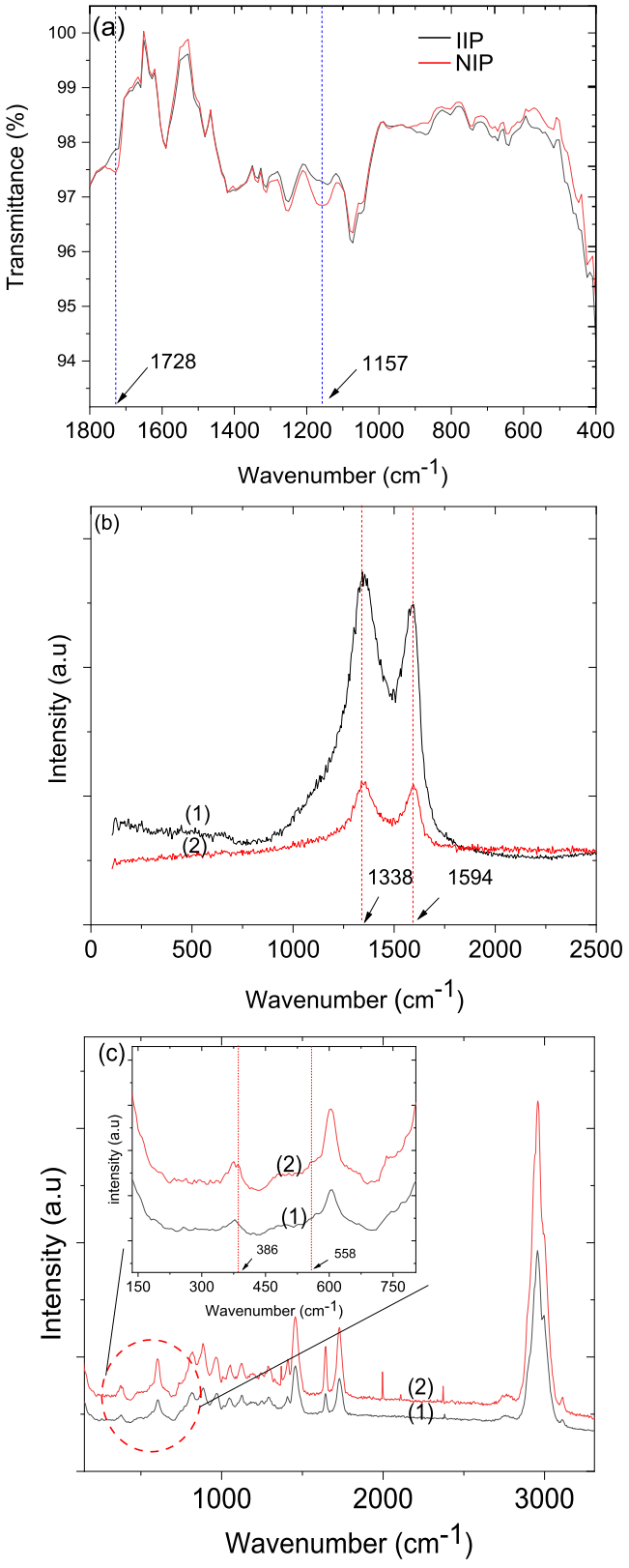

Figure 1. (a) FTIR spectra in the spectral range 1800−400 cm^{-1} of unleached IIP and NIP. (b) Raman spectra of (1) GO and (2) rGO and (c) (1) NIP and (2) unleached IIP.

of 0.38 nm and a peak of 2θ = 43.5°, which confirms the graphitic nature of the rGO.[24]

2.1.4. Brunauer−Emmett−Teller Analysis. Brunauer−Emmett−Teller analysis studies were adopted to evaluate the surface area of leached IIP and unleached IIP at the macro level. A specific pore volume and diameter of the imprinted polymers were determined using the Barrett−Joyner−Halenda N_2 adsorption/desorption isotherm method. The isotherms of the leached IIP and unleached IIP microspheres are presented in Figure 3a,b. The nature of the adsorption/desorption isotherms classified imprinted polymers as type IV with H3 hysteresis loops according to the recommendation of the International Union of Pure and Applied Chemistry classification of isotherms. Therefore, the imprinted polymers possessed a mesoporous structure.[25,26] The pore size distribution (total pore volume and average pore width), as well as the surface area, were calculated from the adsorption/desorption isotherm methods (see the Supporting Information Table S1). It could be seen that the surface areas of unleached IIP and leached IIP were 79.3 and 106 $m^2\ g^{-1}$, respectively, and the average pore widths of unleached IIP and leached IIP were 12.3 and 12.7 nm, respectively. The characteristic physical parameters of imprinted polymers were significantly reduced in unleached IIP. The observation indicated that leached IIP with excessive nanopore and surface area were conveniently synthesized.[27] The template removal created recognition cavities with a complementary spatial structure for selective recognition of Pb(II) in water using leached IIP. The lesser surface area of unleached IIP is ascribed to a confined shrinkage of the pores by the presence of template ions.[26,27]

2.1.5. Scanning and Transmission Electron Microscopic Analysis. The surface morphologies of the synthesized material hybrids were studied using SEM and TEM techniques. The SEM and TEM images of leached IIP, unleached IIP, NIP, and IIP−rGO polysulfone composite are presented in Figure 4. The SEM image displays a highly microporous leached IIP (Figure 4a) with the surface area and pore width of 106 $m^2\ g^{-1}$ and 12.7 nm, respectively, as revealed from adsorption/desorption studies. The ordered nanoporous pattern of leached IIP is probably due to the removal of imprinted Pb^{2+} on the polymer's surface. The nonconformational structure of unleached IIP (Figure 4b) may be attributed to the presence of monomer−template interaction. The micrograph of NIP (Figure 4c) displayed a compacted surface that did not possess the compatible cavities for Pb^{2+} binding in water. The IIP−rGO (Figure 4d) displayed porous IIP packed between rGO layers with residues of polysulfone membrane. However, in the TEM image, these rGO sheets (Figure 4h) were coated on the surface of leached IIP. Scanning electron micrograph images complemented the TEM morphological surface of the synthesized material hybrids. The structural and surface morphological studies of characterization techniques support each other and confirmed the successful preparation of the IIP−rGO and NIP−rGO nanocomposites.

2.2. Chemoresistive Sensor Response and Performance. Three IIP−rGO-based sensors with a mass ratio composition of IIP−rGO of 1:1, 1:2, and 1:3 with polysulfone were prepared. Their performance in $\Delta R/R_o$ responses was recorded at variable concentrations of Pb^{2+} ions in aqueous media at room temperature. The NIP−rGO-based sensor was used in the reference experiment under the same conditions as IIP−rGO. During the measurement, the sensor's contact time with the solution containing Pb^{2+} ions was set to be 15 min all the time for all the sensors. During this time, the metal ions rebound to the cavity of IIP, resulting in the $\Delta R/R_o$ (where

https://doi.org/10.1021/acsomega.1c03955
ACS Omega 2021, 6, 31528−31538

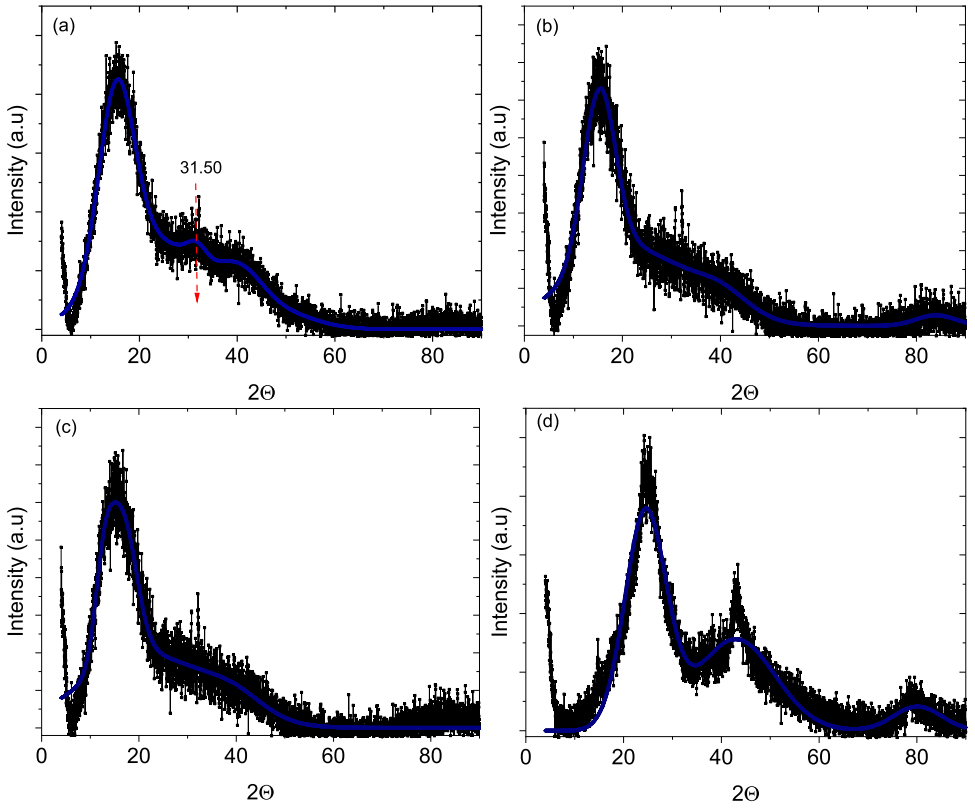

Figure 2. P-XRD and deconvoluted diffraction patterns of (a) unleached IIP, (b) NIP, (c) leached IIP, and (d) rGO.

$\Delta R = R - R_o$, R is the instantaneous resistance of the sensor in Pb^{2+} ions solution and R_o is the resistance of the sensor immersed into leaching solution) of the individual peaks increasing rapidly. When the sensor is removed from the analyte solution and immersed in the 0.16 mM ethylenediaminetetraacetic acid (EDTA) leaching solution for 10 min, the peaks quickly return to the baseline due to Pb^{2+} desorption from the IIP cavities leading to a sensor's regeneration for subsequent analysis. The occurrence of the mechanism because the binding of Pb^{2+} ions to the cavity of IIP−rGO causes an increase in $\Delta R/R_o$ while removal of Pb^{2+} ions from the cavity reduces the sensor's response. The $\Delta R/R_o$ of all of the fabricated sensors was recorded as the function of time with variable concentrations. Figure 5a−f shows the $\Delta R/R_o$ response of the IIP−rGO-based sensors with 1:1, 1:2, and 1:3 mass ratios as a function of the concentration in the solution.

At a lower concentration of rGO in the composites, the mass ratio of 1:1 showed an inconsistent response as the concentration increases from low to high. However, in the 1:2 mass ratio, which has twice the amount of rGO than that in the 1:1 composite, significantly changed in $\Delta R/R_o$ as the Pb^{2+} ion concentration in the solution increased. The 5 and 20 μg L^{-1} peaks (Figure 5c) never reached a plateau and the response slowly descended (descending triangle type peak) until the sensor was removed from the analyte solution and immersed in the leaching solution. The remaining peaks reached plateaus with an equal response magnitude because all readily available active cavities were occupied with Pb^{2+} ions. It is worth noting that as the concentration increased, the rate of response became constant and stagnant from 50−200 μg L^{-1} (Figure 5c,d). Interestingly, when the amount of rGO in the polymer composite was further increased to 1:3, which is 3 times that of 1:1, the sensor showed excellent performance (Figure 5e,f). The exponential decay relationship between the $\Delta R/R_o$ and the concentration of Pb^{2+} ions in aqueous solutions was achieved for the mass ratio of 1:3 reached by increasing the rGO in the polymer composite. This improvement in the sensor's performance is due to the increase in the transfer rate of carriers through the conductive channels by adding more rGO and improving the IIP evenly to contact with rGO. Furthermore, more cavities become available to allow the Pb^{2+} ions to quickly diffuse to the electrode surface and be re-implanted in the cavity.[28] Any further addition of the rGO in the composites, such as 1:4 and 1:5 mass ratios, did not show a progressive decrease in resistance as the concentration increased (not shown here), instead, the inconsistency and nonplateau peaks might be due to the blocking of the active site of the IIP by the excess of rGO.

The peaks for the sensors based on IIP−rGO in 1:3 mass ratio showed a plateau for every contact with the solution, except a slight inclination for 5 and 20 μg L^{-1} concentrations. This suggests that the maximum accessible cavities and conductive channels were achieved from the concentrations of 50−200 μg L^{-1} of the Pb^{2+} ions. Thus, increasing the concentration to 200 μg L^{-1} led to the decrease in the peaks, confirming that the $\Delta R/R_o$ response is inversely proportional to the concentration. When the sensor based on IIP−rGO in 1:3 mass ratio was further analyzed for the curve-fitted (eq 1) exponential decay curve, we found the upper limit of $\Delta R/R_o$ detection to be

$$y = A_1 e^{(-C/C_1)} + y_0 \quad (1)$$

https://doi.org/10.1021/acsomega.1c03955
ACS Omega 2021, 6, 31528−31538

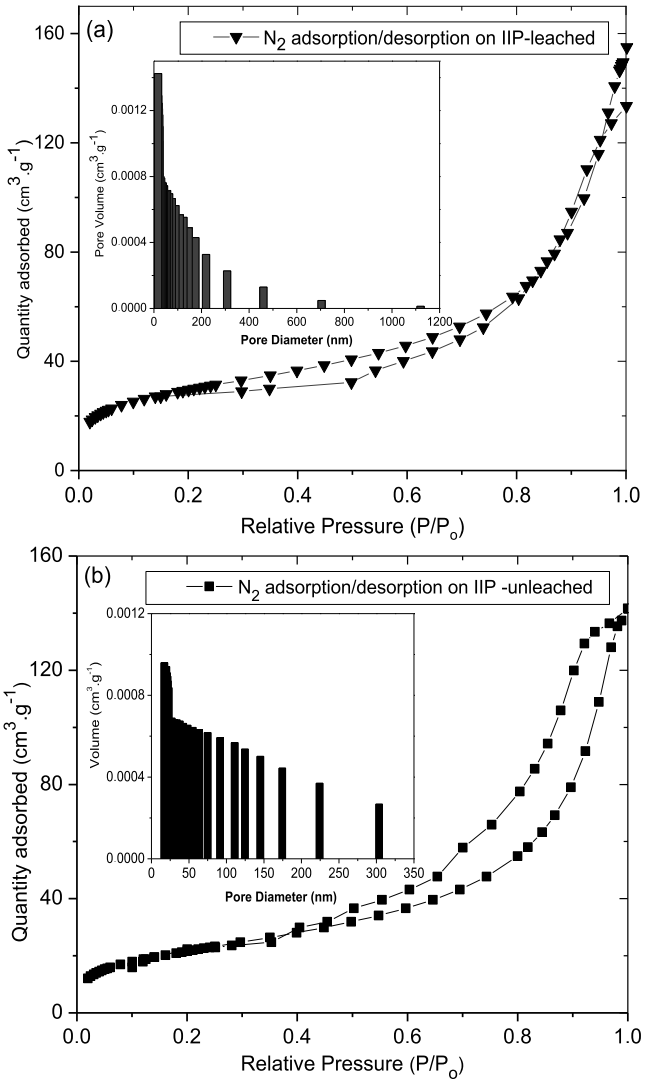

Figure 3. Adsorption/desorption isotherm microsphere of (a) leached IIP (b) unleached IIP.

where A_1 is the pre-exponential constant, 5.2635; C_1 is the concentration constant, 40.0696 μg L^{-1}; and y_o is the offset relative response, 1.7287. Rearranging eq 1

$$\frac{(y - y_o)}{A_1} = e^{(-C/C_1)} \tag{2}$$

By taking the ln function on both sides,

$$\ln\left(\frac{(y - y_o)}{A_1}\right) = \frac{-C}{C_1} \tag{3}$$

Equation 3 is valid only when $y > y_o$; therefore, any given $\Delta R/R_o$ greater than 1.7287 should be valid for the above equation. If $y > y_o$ only by 0.0001, for example, the sensor's upper limit is 436 μg L^{-1}. By taking the logarithmic function of the y- and x-axis of Figure 5f inset, exhibited good linearity with a regression equation of $y = 1.054 - 0.242*X$, coefficent of determination (R^2) = 0.9737, and the LOD was calculated to be 1.77 μg L^{-1}.

On the other hand, the small relative response for the NIP−rGO-based sensor was observed and remained constant despite the change in Pb^{2+} concentration from 5 to 200 μg L^{-1}. This small change in response might be due to the physical adsorption of the Pb^{2+} ions on the surface. The comparison of the IIP- and NIP-based sensors (Figure 8c) shows that there is a significant difference in responses of the IIP- and NIP-based sensors toward Pb^{2+} ions in the solution due to the availability of active cavities on the IIP. Furthermore, the response ratio of the IIP-based sensor to NIP-based sensor $(\Delta R/R_o)_{IIP}/(\Delta R/R_o)_{NIP}$ as a function of the concentration of Pb^{2+} ions in the solution shows that the response ratio recorded a maximum $\Delta R/R_o$ response of approximately 2.0 for NIP and 4.0 for IIP at 50 μg L^{-1}. The ratio decreases as the concentration increases (see Figure 6d) and follows an exponential decay function with the minimum ratio of 2.09 at 200 μg L^{-1}. Interestingly, the $(\Delta R/R_o)_{IIP}/(\Delta R/R_o)_{NIP}$ never reaches 1, which means that both sensors never have the same relative responses. The logarithmic function of the y- and x-axis showed good linearity (see Figure 6d, inset).

2.3. Stability and Reproducibility Test. The stability of the sensor was evaluated using a newly prepared sensor with a 20 μg L^{-1} Pb^{2+} solution. The sensor showed excellent stability and reproducibility during five consecutive contacts with the solution, followed by leaching out the Pb^{2+} ions (Figure 6e). A 90% repeatability of the $\Delta R/R_o$ response was achieved in a consecutive test. The excellent precision calculated as the percentage relative standard deviation of 4.7% of the obtained repeatability is within the acceptable range of the United States Environmental Protection Agency (US EPA) recommendations for assessing the proposed method's precision.[8]

2.4. Selectivity Studies. Selectivity is a vital feature for method validation because it measures a method's ability to measure an analyte accurately in the presence of interferences. The bivalent cations Mn^{2+}, Fe^{2+}, Sn^{2+}, and Ti^{2+} possess ionic charge distribution and size of ionic radii that are closely related to that of Pb^{2+}. These metal ions can compete with Pb^{2+} detection since they usually coexist in the real water samples' matrix component. The interference test was performed by exposing the sensor based on IIP−rGO in 1:3 mass ratio to measure the $\Delta R/R_o$ of the sensor toward each ion with a concentration of 200 μg L^{-1} and mixed metal ions (each metal ions with 200 μg L^{-1}) as a function of time (Figure 7). The individual $\Delta R/R_o$ of competing ions was relatively low compared to that of the target analyte Pb^{2+} ions except for Ti^{2+} ions. Although the response of mixed metal ions was higher than that of the Pb^{2+} ion solution, the ICP-MS analysis of the total metal ions adsorbed by the polymer composite of the sensing material with IIP−rGO in 1:3 mass ratio revealed a surprising result. The IIP−rGO-based sensors selectively adsorbed 93% of the Pb^{2+} ions compared with other metal ions (see the Supporting Information Table S2). This indicates that the increase in $\Delta R/R_o$ of the sensor when exposed to the mixed metal ions might be a contribution from computing ions, which were adsorbed very little. It is further confirmed that a substantial $\Delta R/R_o$ toward recognition of Pb^{2+} ions is due to the imprinting of the cavities with the template ion's specific shape and size.[11] Therefore, IIP−rGO-based sensor is highly selective and reliable toward the detection of the Pb^{2+} ions.

2.5. Analytical Application. The exceptional performance quantities of analytical figures of merit evidenced that sensors based on IIP−rGO in 1:3 molar ratio had high stability, repeatability, and selectivity. An optimal linear curve response of R^2 value of 0.9737, resistive sensitivity of 0.242 $(\mu g\ L^{-1})^{-1}$, and LOD of 1.77 μg L^{-1} was exceptional for the validation of the method. The accuracy of the method was evaluated by

https://doi.org/10.1021/acsomega.1c03955
ACS Omega 2021, 6, 31528−31538

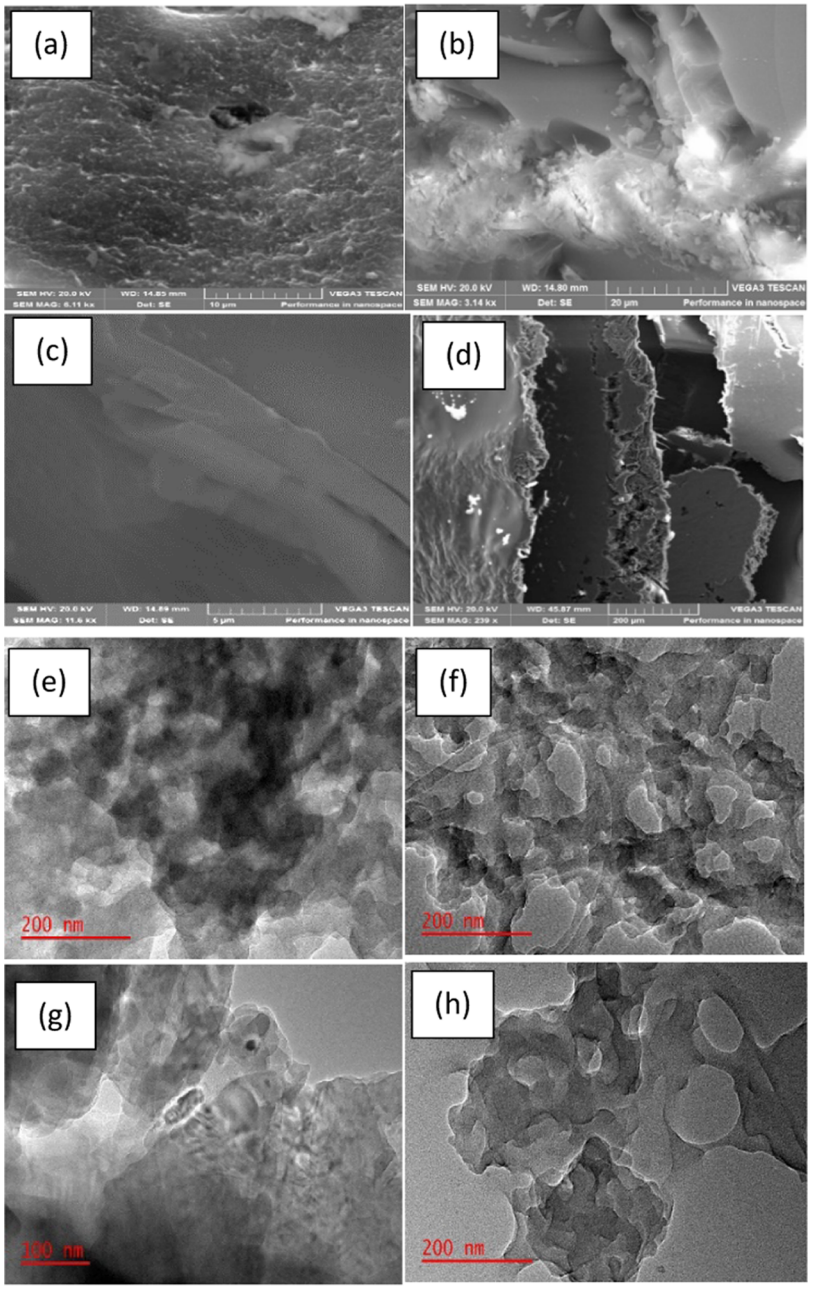

Figure 4. SEM images of (a) leached IIP, (b) unleached IIP, (c) NIP, and (d) IIP−rGO. TEM images of (e) leached IIP, (f) unleached IIP, (g) NIP, and (h) IIP−rGO polysulfone composite.

spiking a real water sample with 200 μg L^{-1} of Pb^{2+} solution. The obtained percentage recovery of 78% complies with US EPA mandatory guidelines for method development and validation, confirming the efficiency of the sensors based on IIP−rGO.[8] The accuracy determination and method validation were performed in triplicate, which showed acceptable stability at 90% repeatability with high selectivity for detection of Pb^{2+} ions in the real sample using the IIP−rGO sensor-based method. Conversely, EDTA's suitability to leach analyte on the sensing layer's recognition cavities was tested experimentally in triplicate. The test solution with 1 mg L^{-1} Pb^{2+} ions was exposed to a sensitive layer under the optimized contact time and leaching conditions. The concentration of leached Pb^{2+} ions of 0.827 ± 0.064 mg L^{-1} determined in the EDTA solution using ICP-AES showed that EDTA was efficient in leaching out the Pb^{2+} ions from the sensor's recognition cavities. A sensor was used for days without degradation in detection ability. Nonetheless, renewability was performed by placing a sensor in the EDTA solution overnight and rinsing it before use.

To the best of our knowledge, a wide variety of studies reported for sensor detection of Pb^{2+} in water inherited various electrochemical, optical, and electrical sensing techniques using different types of chemically modified materials. The trend in the chemical sensing technology incorporates various chemically modified fabricated sensors for the detection of metal ions in water samples.[29] The various fabricated sensors and detection techniques reported in the studies outline the detection of Pb^{2+} in water samples (see the Supporting Information Table S3). Luo et al.[13] reported the preparation of

https://doi.org/10.1021/acsomega.1c03955
ACS Omega 2021, 6, 31528−31538

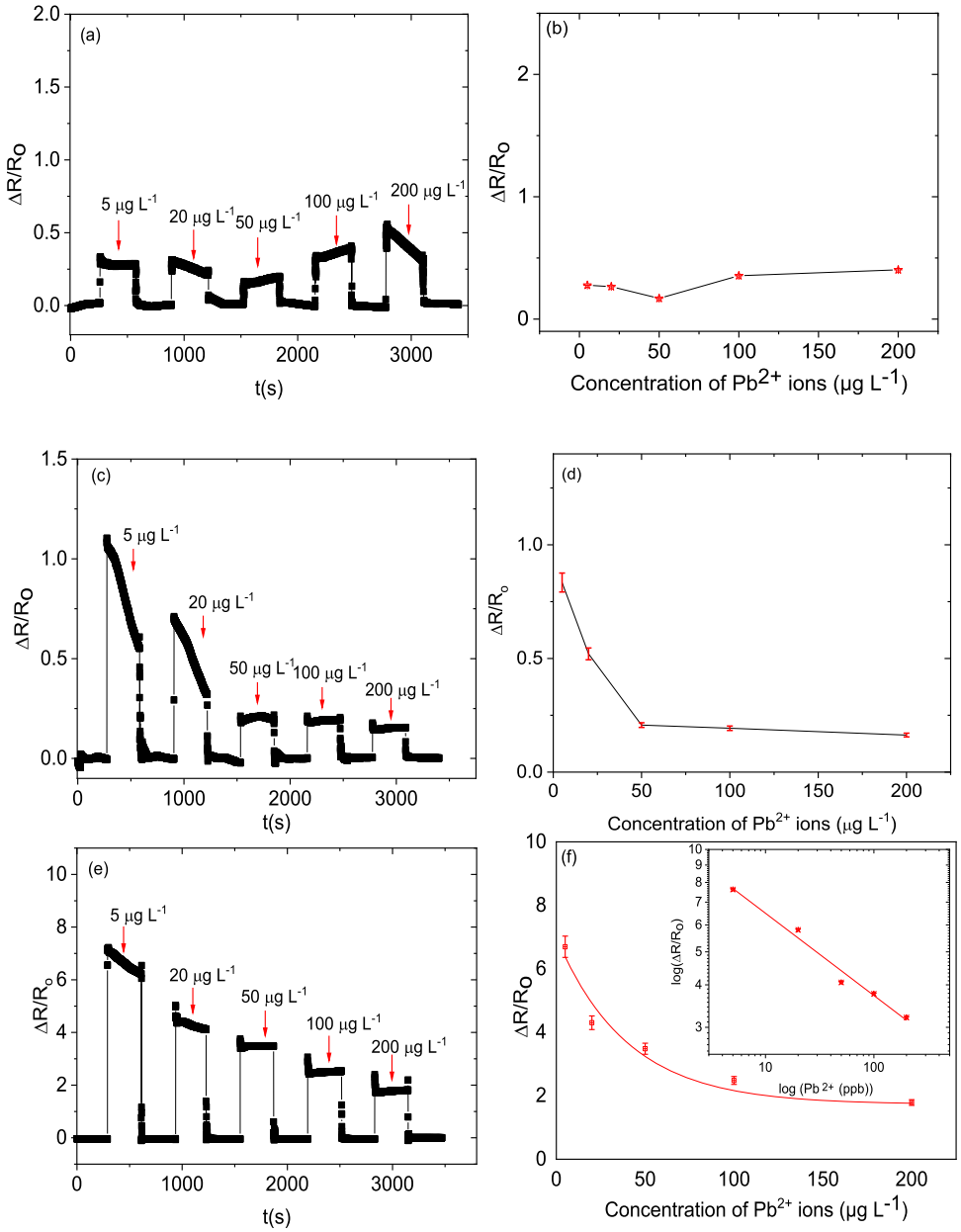

Figure 5. Dynamic response-recovery curve $\Delta R/R_o$ as a function of time (a) and (b) of the 1:1, (c) and (d) of the 1:2, and (e) and (f) of the 1:3 mass ratio of IIP−rGO vs concentration.

the self-manufactured Pb^{2+}-selective electrode using Pb^{2+}-IIPs for differential pulse voltammetry detection. Baghayeri et al.[14] outlined the use of glassy carbon electrode coated with poly(amidoamine) dendrimer functionalized magnetic GO for the simultaneous detection of Pb^{2+} and Cd^{2+} in environmental waters using the square wave anodic stripping voltammetry method in a closed-circuit mode. Recently Sarmiento et al.[30] reported a chemical vapor deposition−conductive reduced GO coated films for electrochemical and electrical detection of Pb^{2+} ions using both cyclic voltammetry and electrical conductance. The novelty of our study was exhibited by the chemoresistive performance of the IIP−rGO-based sensor for the detection of Pb^{2+} ions, which made a significant contribution to the chemical sensing technology. The performance characteristic of the IIP−rGO-based sensor possesses remarkable advantages such as high selectivity, low cost, and high sensitivity toward the detection of Pb^{2+} ions and is comparable with the related studies.[31] Remediation studies integrated into the chemical sensing of metal ions for fabricating chemically modified nanomaterials that are economical, effective, and efficient for metal ions adsorption in the environmental water are growing exponentially.[32−37]

3. CONCLUSIONS

A novel chemoresistive sensor based on IIP−rGO in 1:3 mass ratio for the rapid detection of Pb^{2+} in water relative to relative resistance response using an LCR meter was successfully developed. The synthesized and modified material hybrids, unleached IIP, leached IIP, NIP, GO, rGO, IIP−rGO, and NIP−rGO, were characterized using different analytical techniques. The optimal sensitivity, linearity, stability, LOD, and selectivity features have distinguished the sensor based on IIP−rGO in 1:3 mass ratio as a cost-effective and convenient method with remarkable matrix effect tolerance. The sensor

https://doi.org/10.1021/acsomega.1c03955
ACS Omega 2021, 6, 31528−31538

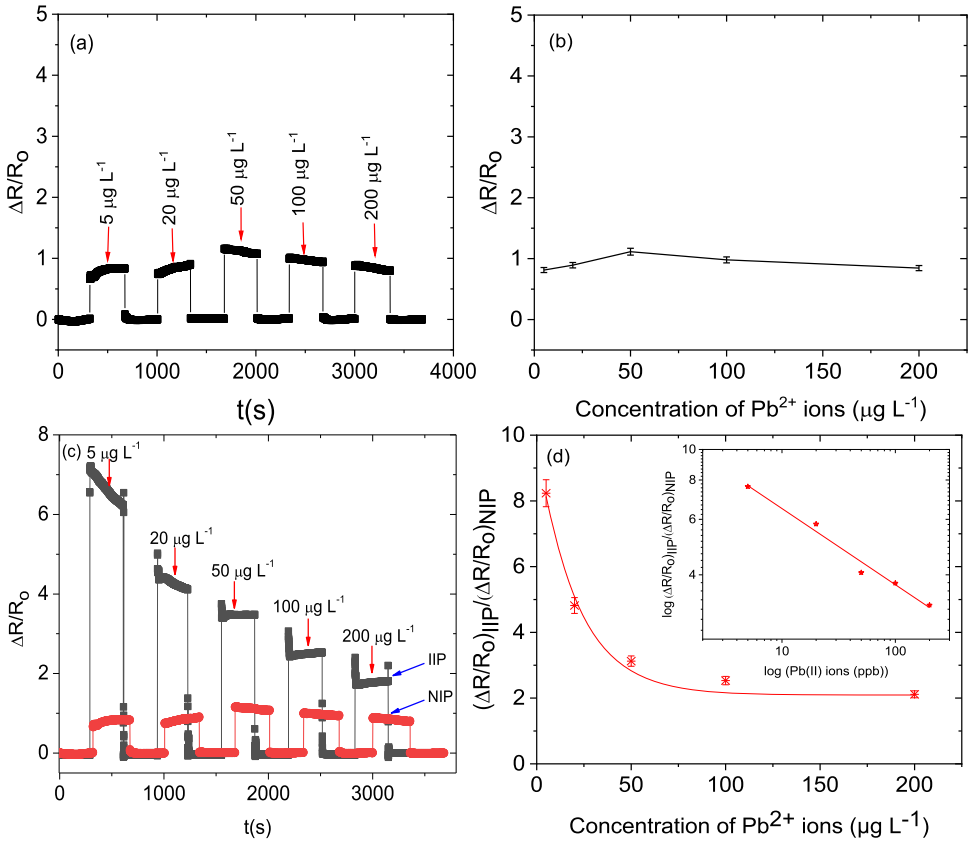

Figure 6. Dynamic response-recovery curve $\Delta R/R_o$ response as a function of time at variable concentrations for (a) NIP−rGO-based sensor of 1:3 mass ratio and (b) $\Delta R/R_o$ response as a function of concentration for NIP−rGO-based sensor of 1:3 mass ratio. (c) Comparative combined graphs of $(\Delta R/R_o)_{IIP}$ and $(\Delta R/R_o)_{NIP}$ with at variable concentrations. (d) Response ration of $(\Delta R/R_o)_{IIP}/(\Delta R/R_o)_{NIP}$ as a function of the concentration with curve fitting.

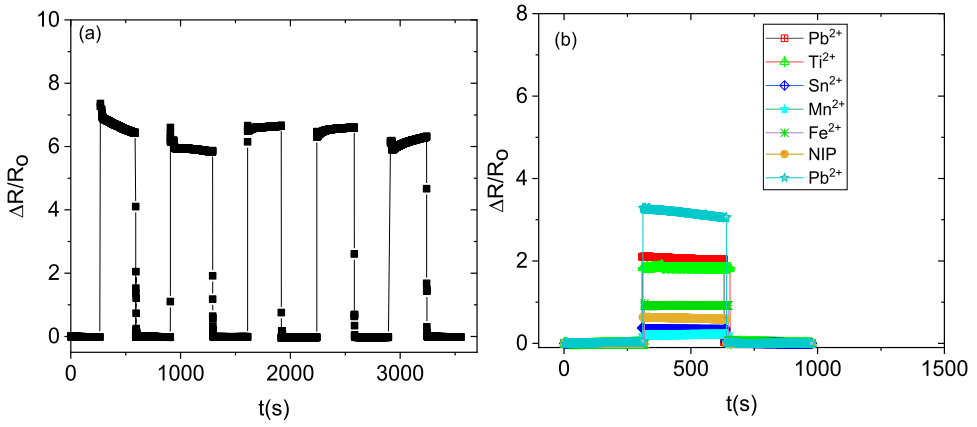

Figure 7. (a) Stability and reproducibility test on 1:3 IIP−rGO-based sensor at 20 μg L^{-1} Pb^{2+} ions. (b) ΔR response as a function of time for IIP−rGO and NIP−rGO-based sensors for evaluating competing ions on recognition of a target analyte Pb^{2+}.

with a 1:3 mass ratio was able to detect Pb^{2+} ions in concentrations as low as 1.77 μg L^{-1} and as high as 436 μg L^{-1}. The sensor based on NIP, however, did show low relative response in a wide range of concentrations with almost the same magnitude. The ratio of the $\Delta R/R_o$ of the IIP to NIP $((\Delta R/R_o)_{IIP}/(\Delta R/R_o)_{NIP})$ as a function of the concentration revealed that both sensors never give the same reading for any given concentration. Thus, a sensor is recommended for the detection of Pb^{2+} ions in real water samples. A bulk polymerization imprinting technology produced ion-imprinted polymer hybrids and incorporating rGO as a nanofiller to leached IIP synergically improved the aggregation of a polymer and amplified a sensing layer's relative resistance performance.

4. MATERIALS AND METHODS

4.1. Chemicals and Reagents. Analytical grade chemicals and reagents were purchased from Merck unless stated otherwise. Ultrapure water obtained from Supre2Pure Milli-Q-system (ThermoScientific) with a resistivity of 18.2 MΩ cm was used to prepare solutions. All glassware was sterilized in dilute nitric acid (HNO_3) solution prepared from 55% HNO_3. The IIP and NIP particles were synthesized and purified using

https://doi.org/10.1021/acsomega.1c03955
ACS Omega 2021, 6, 31528−31538

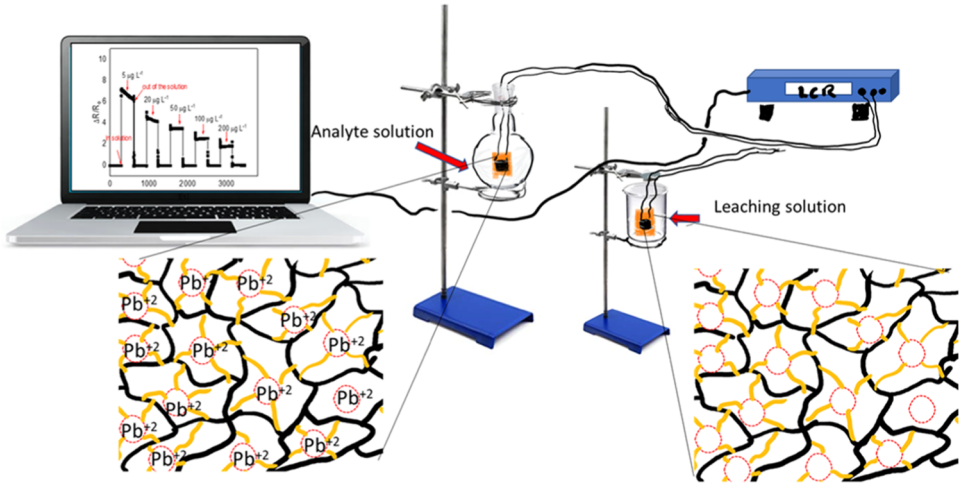

Figure 8. Setup representation of sensor-based method application.

98.0% ethylene glycol dimethyl acrylate (EGDMA), 99% methacrylic acid (MAA), 99.9% dimethyl sulfoxide (DMSO), 99.9% acetonitrile (ACN), 99.0% lead(II) nitrate ($Pb(NO_3)_2$), 94.0% benzoyl peroxide (BPO), 98.5% ethylenediaminetetraacetic acid disodium (EDTA-Na2), and 97.2% ethanol (EtOH). The rGO was synthesized using graphite, 95.0−98.0% sulfuric acid (H_2SO_4), 85% phosphoric acid (H_3PO_4), 99.0% potassium permanganate ($KMNO_4$), 30% hydrogen peroxide (H_2O_2), and 99.0% ascorbic acid ($C_6H_8O_6$). Polymer nanocomposites IIP−rGO and NIP−rGO were synthesized using 99.8% dichloroethane (CH_3CHCl_2) and polysulfone membrane (average M_w ∼35 000). High-purity standard solutions of Pb, Fe, Mn, Sn, and Ti (1000 μg mL^{-1}) were used for sensitivity and selectivity determination and purchased from Inorganic Ventures.

4.2. Characterization and Detection Techniques. The synthesized material hybrids (leached IIP, nonleached IIP, NIP, GO, rGO, IIP−rGO, NIP−rGO) were characterized using Infrared Affinity Fourier transform infrared (FTIR) spectrometer (Shimadzu, Germany) with a resolution of 4.0 cm^{-1} within 400−4000 cm^{-1} wavenumber range, Witec 300 Confocal Laser Raman spectroscopy (Witec Focus Innovations, Germany) with charge-coupled device detector from a pixel of 0−4000 cm^{-1} Raman shift, Rigaku MiniFlex 600 powder X-ray (P-XRD) diffractometer (MiniFlex, Germany) with a Cu Kα (λ = 1.54056 nm) radiation source, ASAP 2460 Micromeritics surface and porosity analyzer (Micromeritics Instrument Corporation) for nitrogen (N_2) adsorption/desorption experiment and morphological studies using Joel-Jem 7500F scanning electron microscopy (SEM) (Joel, Japan) and Joel-Jem 2100F transmission electron microscopy (TEM) (Joel, Japan). Electrical characterization of IIP−rGO- and NIP−rGO-based sensors was performed using an ISOtech 821 LCR meter. Daily calibration of the LCR meter was performed using a known resistor and capacitor confirmed with 34461A Bench Digital Multimeter (Keysight Technologies, Malaysia). Analyte concentration determination was performed using ICPE-9800 Series ICP-AES (Shimadzu, Japan) and Sciex Elan 6100 ICP-MS (Perkin Elmer, Germany).

4.3. Experimental Methods. *4.3.1. Synthesis of Pb^{2+}Ion-Imprinted Polymers.* The Pb^{2+}-IIP unleached was synthesized by bulk polymerization procedure using 4 mM monomer MAA, 20 mM cross-linker EDGMA, 0.3 mM initiator BPO, and (1:9 v/v) DMSO/ACN in the presence of 0.5 mM $Pb(NO_3)_2$.[1717] Briefly, 0.5 mM amount of $Pb(NO_3)_2$ was dissolved in 10 mL of porogen mixture in the reaction flask to generate Pb^{2+} template ions. A monomer and cross-linker were then added to the reaction flask and stirred, sealed for 10 min at room temperature, followed by an appropriate amount of BPO, and stirred until completely dissolved. The reaction mixture purged for 10 min with N_2 to create an inert atmosphere. A reaction flask was sealed with aluminum foil and parafilm and set for polymerization on a thermostat oil bath at 60 °C for 24 h under vigorous stirring. The NIP control material was prepared following the same procedure except without the template ion (Pb^{2+}). Then, the final product was finely ground and sieved through a 45 μm wire mesh to collect materials with uniform micron-sized particles. Imprinted polymers were purified in an EtOH solution and repeatedly rinsed with ultrapure water. A portion of dried unleached Pb-IIP was treated with 13.5 mM EDTA solution at several cycles to extract Pb^{2+} templated ions. Aliquots of extracted solutions were analyzed with ICP-AES until Pb^{2+} ions were not detected. The resulting leached IIP, as well as unleached IIP and NIP, were characterized using various techniques. The leached IIP and NIP were taken further for the synthesis of polymer nanocomposites.

4.3.2. Synthesis of Reduced Graphene Oxide Imprinted Polymer for the Fabrication of Sensors. The rGO was used as a reinforcing material in the synthesis of conductive nanocomposites prepared using graphite as a starting material to synthesize graphene oxide (GO). The GO was synthesized by modifying the Staudenmaier and Hummers method, as reported by Kibechu et al.[10] Briefly, 3 g of graphite flakes were transferred into a 1000 mL round-bottom flask placed in the ice bath. Cautiously, H_2SO_4/H_3PO_4 (9:1 v/v) was added into the flask by allowing 360 mL of H_2SO_4 to cool while stirring, followed by the addition of 40 mL of H_3PO_4. Eighteen grams of $KMNO_4$ was added slowly in 2 min intervals, while the reaction was stirred for 30 min. The mixture was heated in an oil bath for 24 h under stirring. After cooling, 3% H_2O_2 was slowly added to the mixture to react with unreacted $KMNO_4$. The mixture was sonicated for 2 h to exfoliate GO layers, thus forming a brown solution. Graphene oxide solution was filtered using membranes of 0.45 μm pore size and centrifuged continuously using ultrapure water until the supernatant solution was weakly acidic (pH 5) and dried in an oven for characterization. An amount of 0.5 g of GO was added to a

https://doi.org/10.1021/acsomega.1c03955
ACS Omega 2021, 6, 31528−31538

reaction flask containing 1.0 g of ascorbic acid and 250 mL of ultrapure water and ultrasonicated for 30 min. A reaction flask was continued to be stirred in an oil bath at 80 °C for 24 h to synthesize rGO, which was then rinsed repeatedly with ultrapure water and dried in an oven.

4.3.3. Fabrication of Sensors. The leached IIP and NIP materials were loaded with rGO to form polymer nanocomposites by the solution mixing process. Two hundred milligrams of polysulfone dissolved was in 5 mL of dichloroethane, and 10 mL of solution was added to a mixture of 0.02 g of leached IIP and 0.04 g of rGO (1:2 w/w) and the two solutions were mixed. The polysulfone binds together the synthesized IIP and rGO on the interdigitated electrode (IDE). A similar procedure was followed for the synthesis of a control polymer. The reaction mixture was ultrasonicated and continued to be stirred for a minimum of 48 h to form a homogeneous polymer nanocomposite solution IIP−rGO and control NIP−rGO. The polymer nanocomposites solutions were drop-cast onto gold IDE to create a thin film and dried under a vacuum desiccator.

4.3.4. Characterization of the Fabricated Sensors. The response of a chemoresistive IIP−rGO-based sensor toward Pb^{2+} in the test solution was measured using an ISOTECH LCR 821 LCR meter at an AC input signal of 0.5 V amplitude and 25 kHz frequency,[18] with the resistance measured as the output signals. The setup representation of the IIP−rGO-based sensor application for detecting Pb^{2+} in a test solution using an LCR meter is presented in Figure 8. As illustrated, an IIP−rGO-based sensor was exposed to Pb^{2+} concentrations in a test solution prepared for 15 min, then the sensors were rinsed and exposed to 0.16 mM EDTA leaching solution for 10 min. The sensor was rinsed before the next measurement. The NIP−rGO-based sensor response performed a control experiment. The contact time and leaching time were kept constant for the optimization of all measurements.

■ ASSOCIATED CONTENT

Supporting Information

The Supporting Information is available free of charge at https://pubs.acs.org/doi/10.1021/acsomega.1c03955.

Contains tables of nitrogen adsorption−desorption studies of results of unleached IIP and leached IIP, the result of ICP-MS analysis of the leached solution from IIP−rGO-based sensor after exposure to mixed metal ion solution, and a comparative table of previously reported IIP-based Pb^{2+} sensors with references (PDF)

■ AUTHOR INFORMATION

Corresponding Author

Messai A. Mamo − *Department of Chemical Science, Faculty of Science, University of Johannesburg, Johannesburg 2028, South Africa;* orcid.org/0000-0002-6734-2051; Email: messaim@uj.ac.za

Authors

Mokgehle R. Letsoalo − *Department of Chemical Sciences, Faculty of Science, University of Johannesburg, Johannesburg 2028, South Africa*

Abayneh A. Ambushe − *Department of Chemical Sciences, Faculty of Science, University of Johannesburg, Johannesburg 2028, South Africa;* orcid.org/0000-0001-8763-8346

Complete contact information is available at: https://pubs.acs.org/10.1021/acsomega.1c03955

Author Contributions

The manuscript was written through the contributions of all authors.

Notes

The authors declare no competing financial interest.

■ ACKNOWLEDGMENTS

This work is based on the research supported in part by the National Research Foundation (NRF) of South Africa under the Thuthuka Programme Grant Number 117673 and the Water Research Commission (WRC) of South Africa Project Number K5/2515//1. The authors would like to acknowledge the University of Johannesburg Research Centre for Synthesis and Catalysis and Spectrum for the facility. M.R.L. is grateful to the DST-NRF Innovation Doctoral scholarship and University of Johannesburg Global Excellence and Stature scholarship for financial support.

■ REFERENCES

(1) Zhu, X.; Cui, Y.; Chang, X.; Zou, X.; Li, Z. Selective Solid-phase Extraction of Lead(II) From Biological and Natural Water Samples Using Surface-grafted Lead(II)-imprinted polymers. *Microchim. Acta* **2009**, *164*, 125−132.

(2) Shamsipur, M.; Samandari, L.; Besharati-Seidani, A.; Pashabadi, P. Synthesis, Characterization and Using a New Terpyridine Moiety-based Ion-imprinted Polymer Nanoparticle: Sub-nanomolar Detection of Pb(II) in Biological and Water Samples. *Chem. Pap.* **2018**, *72*, 2707−2717.

(3) Verma, R.; Dwivedi, P. Heavy Metal Water Pollution-A case study. *Recent Res. Sci. Technol.* **2013**, *5*, 98−99.

(4) Khan, T.; Mustafa, M. R. U.; Isa, M. H.; Manan, T. S. B. A.; Ho, Y.-C.; Yusof, N. Z. Artificial Neural Network (ANN) for Modelling Adsorption of Lead (Pb (II)) from Aqueous Solution. *Water, Air, Soil Pollut.* **2017**, *228*, No. 426.

(5) Biswas, T. K.; Yusoff, M. M.; Sarjadi, M. S.; Arshad, S. E.; Musta, B.; Rahman, M. L. Heavy Metals Removal From Electroplating Wastewater by Waste Fiber-based Poly(amidoxime) Ligand. *Sep. Sci. Technol.* **2019**, *13*, No. 1260.

(6) Pérez-Quintanilla, D.; Sánchez, A.; Hierro, I. D.; Fajardo, M.; Sierra, I. Solid Phase Extraction of Pb(II) in Water Samples Using a New Hybrid Inorganic-organic Mesoporous Silica Prior to Its Determination by FAAS. *Microchim. Acta* **2009**, *165*, 291−298.

(7) Tripathi, A.; Ranjan, M. R. Heavy Metal Removal from Wastewater Using Low-Cost Adsorbents. *J. Biorem. Biodegrad.* **2015**, *6*, No. 315.

(8) World Health Organization (WHO). *Chlorpyrifos in Drinking-Water-Background Document for Preparation of WHO Guidelines for Drinking-Water Quality*; World Health Organization (WHO/SDE/WSH/03.04/87): Geneva, 2003.

(9) Letsoalo, M. R.; Mamo, M. A.; Ambushe, A. A. Simultaneous Quantitative Speciation of Selected Toxic Elements in Water using High Performance Liquid Chromatography Coupled to Inductively Coupled Plasma-mass Spectrometry (HPLC-ICP-MS). *Phys. Chem. Earth* **2020**, No. 103011.

(10) Kibechu, R. W.; Mamo, M. A.; Msagati, T. A. M.; Sampath, S.; Mamba, B. B. Synthesis and Application of Reduced Graphene Oxide and Molecularly Imprinted Polymers Composite in Chemo Sensor for Trichloroacetic Acid Detection in Aqueous Solution. *Phys. Chem. Earth* **2014**, *76*−*78*, 49−53.

(11) Branger, C.; Meouche, W.; Margaillan, A. Recent Advances on Ion-imprinted Polymers. *React. Funct. Polym.* **2013**, *73*, 859−875.

(12) Han, D.; Yan, L.; Chen, W.; Li, W. Preparation of Chitosan/Graphene Oxide Composite Film with Enhanced Mechanical Strength in the Wet State. *Carbohydr. Polym.* **2011**, *83*, 653−658.

(13) Luo, X.; Huang, W.; Shi, Q.; Xu, W.; Luan, Y.; Yang, Y.; Wang, H.; Yang, W. Electrochemical Sensor Based on Lead Ion-imprinted Polymer Particles for Ultra-trace Determination of Lead Ions in Different Real Samples. *RSC Adv.* **2017**, *7*, 16033−16040.
(14) Baghayeri, M.; Alinezhad, H.; Fayazi, M.; Tarahomi, M.; Ghanei-Motlagh, R.; Maleki, B. A Novel Electrochemical Sensor Based on a Glassy Carbon Electrode Modified with Dendrimer Functionalized Magnetic Graphene Oxide for Simultaneous Determination of Trace Pb(II) and Cd(II). *Electrochim. Acta* **2019**, *312*, 80−88.
(15) Nejadmansouri, M.; Majdinasab, M.; Nunes, G. S.; Marty, J. L. Review An Overview of Optical and Electrochemical Sensors and Biosensors for Analysis of Antioxidants in Food during the Last 5 Years. *Sensors* **2021**, *21*, No. 1176.
(16) Jakavula, S.; Biata, N. R.; Dimpe, K. M.; Pakade, V. E.; Nomngongo, P. N. A Critical Review on the Synthesis and Application of Ion-imprinted Polymers for Selective Preconcentration, Speciation, Removal and Determination of Trace and Essential Metals from Different Matrices. *Crit. Rev. Anal. Chem.* **2020**, 1−13.
(17) Kusumkar, V. V.; Galamboš, M.; Viglašová, E.; Daňo, M.; Šmelková, J. Ion-imprinted Polymers: Synthesis, Characterisation, and Adsorption of Radionuclides. *Materials* **2021**, *14*, No. 1083.
(18) Greenshields, M. W. C. C.; Hummelgen, I. A.; Mamo, M. A.; Shaikjee, A.; Mhlanga, S. D.; Van Otterlo, W. A. L.; Coville, N. J. Composites of Polyvinyl Alcohol and Carbon (Coils, Undoped and Nitrogen Doped Multiwalled Carbon Nanotubes) as Ethanol, Methanol and Toluene Vapor Sensors. *J. Nanosci. Nanotechnol.* **2011**, *11*, 10211−10218.
(19) Nchoe, O. B.; Klink, M. J.; Mtunzi, F. M.; Pakade, V. E. Synthesis, Characterization, and Application of *β*-cyclodextrin-based Ion-imprinted Polymer for Selective Sequestration of Cr(VI) ions From Aqueous Media: Kinetics and Isotherm studies. *J. Mol. Liq.* **2020**, *298*, No. 111991.
(20) Zhao, G.; Ren, X.; Gao, X.; Tan, X.; Li, J.; Chen, C.; Huang, Y.; Wang, X. Removal of Pb(II) ions from aqueous solutions on few-layered graphene oxide nanosheets. *Dalton Trans.* **2011**, *40*, No. 10945.
(21) Krishnamoorthy, K.; Veerapandian, M.; Mohan, R.; Kim, S.-J. Investigation of Raman and Photoluminescence Studies of Reduced Graphene Oxide Sheets. *Appl. Phys. A* **2012**, *106*, 501−506.
(22) Burgio, L.; Clark, R. J. H.; Firth, S. Raman Spectroscopy as a Means for the Identification of plattnerite (PbO_2), of Lead Pigments and of their Degradation Products. *Analyst* **2001**, *126*, 222−227.
(23) Yao, Y.; Huang, C.; Chen, X.; Wei, F.; Feng, H. Preparation and Characterization of a Porous Structure PbO2-ZrO2 Nanocomposite Electrode and Its Application in Electrocatalytic Degradation of Crystal Violet. *J. Electrochem Soc.* **2017**, *164*, E367−E373.
(24) Jayachandiran, J.; Yesuraj, J.; Arivanandhan, M.; Raja, A.; Suthanthiraraj, S. A.; Jayavel, R. D.; Nedumaran, D. Synthesis and Electrochemical Studies of rGO/ZnO Nanocomposite for Supercapacitor Application. *J Inorg. Organomet. Polym. Mater.* **2018**, *28*, 2046−2055.
(25) Yang, S.; Chen, G.; Lv, C.; Li, C.; Yin, N.; Yang, F.; Xue, L. Evolution of Nanopore Structure in Lacustrine Organic-rich Shales During Thermal Maturation From Hydrous Pyrolysis, Minhe Basin, Northwest China. *Energy Explor. Exploit.* **2018**, *36*, 265−281.
(26) Zhang, X.; Jia, W.; Liu, C.; Wang, R.; Li, K.; Li, H.; Chen, C.; Sun, Y.; Ruso, J. M.; Hu, D.; Liu, Z. Study on Synthesis and Adsorption Properties of ReO_4^- Ion Imprinted Polymer. *J. Polym. Res.* **2020**, *27*, No. 201.
(27) Masoumi, F.; Sarabadani, P.; Khorrami, A. R. Synthesis, Characterization and Application of a New Nano-structured Samarium(III) Ion-imprinted polymer. *Polym. Bull.* **2019**, *76*, 5499−5516.
(28) Rong, Q.; Li, K.; Wang, C.; Zhang, Y.; Chen, M.; Zhu, Z.; Zhang, J.; Liu, Q. Enhanced Performance of an Acetone Gas Sensor Based on Ag-$LaFeO_3$ Molecular Imprinted Polymers and Carbon Nanotubes Composite. *Nanotechnology* **2020**, *31*, No. 405701.
(29) Zhou, N.; Chen, H.; Li, J.; Chen, L. Highly Sensitive and Selective Voltammetric Detection of Mercury(II) Using an ITO electrode Modified with 5-methyl-2-thiouracil, Graphene Oxide and Gold Nanoparticles. *Microchim. Acta* **2013**, *180*, 493−499.
(30) Sarmiento, V.; Malcolm Lockett, M.; Sumbarda-Ramos, E. G.; Vázquez-Mena, O. High Performance Pb^{2+} Detection using CVD-produced High Quality Multilayer Reduced Graphene Oxide. *Nano Express* **2021**, *2*, No. 010023.
(31) Ghanei-Motlagh, M.; Taher, M. A.; Heydari, A.; Ghanei-Motlagh, R.; Gupta, V. K. Synthesis and Application of a Novel Nanostructured Ion-imprinted Polymer for the Preconcentration and Determination of Thallium(I) ions in Water Samples. *Mater. Biol. Appl.* **2016**, *63*, 367−375.
(32) Umejuru, E. C.; Prabakaran, E.; Kriveshini, P. Nanocomposite for Rapid Removal of Pb^{2+} Ions and Reuse of Spent Adsorbent for Photocatalytic Degradation of Acetaminophen. *ACS Omega* **2021**, *6*, 11155−11172.
(33) Cai, X.; Li, J.; Zhang, Z.; Yang, F.; Dong, R.; Chen, L. Novel Pb^{2+} Ion Imprinted Polymers Based on Ionic Interaction via Synergy of Dual Functional Monomers for Selective Solid-Phase Extraction of Pb^{2+} in Water Samples. *ACS Appl. Mater. Interfaces* **2014**, *6*, 305−313.
(34) Xu, S.; Chen, L.; Li, J.; Guan, Y.; Lu, H. Novel Hg^{2+} -Imprinted Polymers Based on Thymine−Hg^{2+}−Thymine Interaction for Highly Selective Preconcentration of Hg^{2+} in Water Samples. *J. Hazard. Mater.* **2012**, *237*−*238*, 347−354.
(35) Bojdi, K.; Mashhadizadeh, M. H.; Behbahani, M.; Farahani, A.; Davarani, S. S. H.; Bagheri, A. Synthesis, Characterization and Application of Novel Lead Imprinted Polymer Nanoparticles as a High Selective Electrochemical Sensor for Ultra-trace Determination of Lead Ions in Complex Matrixes. *Electrochim. Acta* **2014**, *136*, 59−65.
(36) Bahrami, A.; Besharati-Seidani, A.; Abbaspour, A.; Shamsipur, M. A Highly Selective Voltammetric Sensor for Sub-nanomolar Detection of Lead Ions using a Carbon Paste Electrode Impregnated with Novel Ion Imprinted Polymeric Nanobeads. *Electrochim. Acta* **2014**, *118*, 92−99.
(37) Hassan, K. M.; Gaber, S. E.; Altahan, M. F.; Azzem, M. A. Novel Sensor Based on Poly (1,2-Diaminoanthraquinone) for Individual and Simultaneous Anodic Stripping Voltammetry of Cd^{2+}, Pb^{2+}, Cu^{2+} and Hg^{2+}. *Electroanalysis* **2018**, *30*, 1155−1162.

https://doi.org/10.1021/acsomega.1c03955
ACS Omega 2021, 6, 31528−31538